Sensing and Bio-Sensing Research 50 (2025) 100885

Contents lists available at ScienceDirect

Sensing and Bio-Sensing Research

journal homepage: www.elsevier.com/locate/sbsr

In-vitro real-time magnetic recording of neuronal activity on spinal cord slices

Arturo Vera [a], Ivo Calaresu [b], Isidoro Martínez [a,c], Rubén Guerrero [d], Denis Scaini [b,e,f], Guillermo de Arana Schoebel [a], Jaime J. Hernandez [a], Isabel Rodríguez [a], Rodolfo Miranda [a,g], Eduardo Daniel Martín [h], Julio Camarero [a,g], María Teresa González [a], Lucas Pérez [a,i,*], Laura Ballerini [b]

[a] Fundación IMDEA Nanociencia, 28049 Madrid, Spain
[b] International School for Advanced Studies (SISSA), 34136 Trieste, Italy
[c] Departamento Física Aplicada a las Ingenierías Aeronáutica y Naval, E.T.S.I. Aeronáutica y del Espacio, Universidad Politécnica de Madrid, 28040 Madrid, Spain
[d] Departamento de Física Aplicada and Instituto de Nanociencia, Nanotecnología y Materiales Moleculares - INAMOL, Universidad de Castilla la Mancha, Avenida Carlos III s/n, 45071, Toledo, Spain
[e] Basque Foundation for Science, Ikerbasque, Bilbao 48013, Spain
[f] Universidad del País Vasco (UPV/EHU), Barrio Sarriena s/n, 48940 Leioa, Spain
[g] Dept. Física de la Materia Condensada, Universidad Autónoma de Madrid, Cantoblanco, 28049 Madrid, Spain
[h] Instituto Cajal, Consejo Superior de Investigaciones Científicas (CSIC), 28002 Madrid, Spain
[i] Departamento de Física de Materiales. Universidad Complutense de Madrid, 28040 Madrid, Spain

ARTICLE INFO

Keywords:
Neural tissue
Spinal cord slices
Real time monitoring
Magnetic sensing
Solid-state sensors

ABSTRACT

Recording the neural activity that originates from action potential dynamics has long been a major pursuit in neuroscience and, specifically, to develop neural interfaces, which are crucial for probing and understanding the nervous tissue. Conventional electrodes and emergent optical imaging (using genetically encoded fluorescence indicators) are complementary technologies to measure neuronal activity in-vivo but present intrinsic and general physical constraints. While optical imaging is difficult to translate in humans due to the strong genetic perturbations it involves, recordings through rigid implanted electrodes get frequently compromised over time by the foreign body reaction of the tissue that hinders the charge transfer to the electrode. In this scenario, magnetic sensing technologies can open further possibilities. Their working principle does not require intimate contact or charge transfer with the neural tissue and allows for well-tested soft polymeric coatings, which can facilitate the long-term functionality of implanted monitoring interfaces. Here, we report on the development of spintronic-based magnetic sensors able to detect neuronal activity emerging from spinal cord slices in physiological conditions at room temperature and with no magnetic shielding. We pharmacologically weaken synaptic inhibition inducing a switch from random to synchronous generation of action potentials, characterized by the appearance of slow-paced bursting in SCSs. The biological nature of the signals recorded was assessed by pharmacological removal of action potentials by tetrodotoxin and also by performing live Ca2+ imaging recordings simultaneously with magnetophysiology. Our results pave the way towards developing implanted devices that detect magnetic fields from neuronal activity for daily life applications.

1. Introduction

The ability to monitor neural signals *in-vivo* holds the key to the understanding of their complex mechanisms and it is needed to develop devices to repair and reconnect damaged neural tissues [1]. The activity of neurons is generated by ionic flows across the cell membrane and can be measured either indirectly, monitoring processes related to electrical activity by fluorescent indicators [2,3], or directly, with appropriate local probes [4]. The electrical recording probes that measure neural activity are either extra or intra-cellular [5]. However, the latter modality is difficult to implement *in-vivo* and, therefore, unsuitable for clinical devices. In the case of extracellular recording, the signal comes from the total voltage arising from the net neuronal activity, and measurements are always done with respect to a reference

* Corresponding author at: Departamento de Física de Materiales. Universidad Complutense de Madrid, 28040 Madrid, Spain.
E-mail address: lucas.perez@ucm.es (L. Pérez).

https://doi.org/10.1016/j.sbsr.2025.100885
Received 12 June 2025; Received in revised form 19 September 2025; Accepted 29 September 2025
Available online 1 October 2025

electrode [6], thus depending on the correct functioning of not only one but two electrodes.

The medical community demands implanted neural interfaces able to record neural activity *in-vivo* with good spatial resolution in daily life situations. Beyond diagnostic applications, this allows for the development of neuroprosthesis [7–9] and brain–machine interfaces [10,11]. In addition, being able to record the neural activity during deep brain stimulations will improve our understanding of the stimulation efficacy and allowing its modulation [10]. These applications need implanted interfaces, which are usually intracortical microelectrodes arrays, with needles inserted within the cortex [12–14] or individual larger electrodes deep in brain [15]. However, these frequently lead to the formation of glial scars that encapsulate the electrodes reducing substantially their signal-to-noise ratio only a few months after implantation [16,17]. Recently, dense three-dimensional electrode arrays for electrophysiology have been validated [18,19] and sufficiently thin interfaces have been shown to improve the stability of the recordings [20], but some of them are still rigid. A significant effort is being made in the research community to move from rigid probes into new ones fabricated on flexible polymeric substrates [21–27]. These materials have also allowed new microfabrication processes aimed to condensate a large number of electrode pads in a small probe [28], including the integration of the reference electrode in a single device. Flexible neural probes greatly reduce the impact of the implant in the neural tissue and have shown very good stability both in vitro and in vivo [29–32]. Despite their improved results respect to rigid interfaces, failures at the electrode pads such as layer cracking, insulation loss, or delamination are still observed in flexible devices after long uses, especially when used for both recording and stimulation [33]. Further improvement can come from nanostructuring the electrode pads that has shown to reduce the electrode impedance and improve the electrode/tissue interaction [34–36].

Magnetic recording probes for neuronal activity could be complementary to electrophysiology. Contrary to electric fields, which strongly depend on the dielectric properties of the tissue between the neuronal sources and the recording electrodes, the magnetic properties of tissue are similar to those of air and, thus, the magnetic field is attenuated only by the distance to the current source [37]. In contrast to voltage measurements, where the recordings yield scalar values, the magnetic field is a vector. Thus, magnetophysiology, the magnetic recording of the magnetic fields generated by currents flowing on cells or biological tissues, provides a more precise and complete scenario of the neuronal activity. Additionally, magnetic detection is reference-free and therefore allows for an unbiased measure of connectivity.

Magnetoencephalography [38] (MEG) is a noninvasive method that measures the magnetic fields of active neuronal populations during perceptual or cognitive tasks using Superconducting Quantum Interference Devices (SQUIDs) cooled down to the temperature of liquid helium (4.2 K). Despite the large sensitivity [39], in the range from femtotesla (10^{-15} T) to picotesla (10^{-12} T), the need for extremely low temperatures for the SQUID operation prevents its use in portable devices. Recently, the development of Optically Pumped Magnetometers (OPM) has helped this technique to achieve similar detectivity values as the SQUID [40]. OPMs are based on the spin exchange relaxation-free (SERF) effect and work by heating a small (less than 1 cm^3 volume) chamber containing the working vapor (alkali atoms) to 60 - 150 °C. This heating constraint is more convenient for implementation than the cryogenic temperatures needed for SQUIDs; therefore, this technology is starting to replace them in MEG studies [41]. Still, the minimum volume of each OPM unit is of the order of several cubic millimeters and the technology for heating the vapor complicates the device, limiting their use to non-invasive applications where the sensors are placed over the skin. Therefore, neither SQUIDs nor OPMs allow for chronic implantation due to all the mentioned issues: they are bulky systems that need to be heated or cooled in a range of temperatures far beyond the one of the human body. While these techniques offer very good sensitivity, their use is therefore limited to non implantable applications.

Because of this, solid-state devices have attracted much attention as they do not have the limitations mentioned above of SQUIDs and OPMs potentially allow implantation and further miniaturization. As they do not need intimate contact with the neural tissue as voltage electrodes, they can be fully covered by soft polymeric coatings that will ensure good chemical and mechanical compliance with the neural tissue, hopefully leading to long-term recordings. Recent studies have demonstrated the capability to read magnetic signals from different neural tissues using sensors based on Giant Magnetoresistance (GMR) [42]. However, additional effort is needed for the development of a portable device able to work in real-time without any magnetic shielding. Additionally, the development of novel in-vitro neural sensing technologies may aid in creating multi-physics platforms that can significantly enhance sensitivity and signal resolution for biosensing applications [43] .

In this paper, we report on the detection of neural magnetic fields from spinal cultured explants at room temperature, using a noninvasive configuration. The magnetic recordings are reference-free and the use of a secondary sensor that records only environmental background signals allows to carry out the detection of very small signals without magnetic shielding. We have measured neural activity without the need for electrical stimulation of the neural tissue and without any digital post-processing or time-series averaging.

2. Results and discussion

Tunnel magnetoresistance (TMR)-based magnetic sensors were used as sensing elements. We used polydimethylsiloxane (PDMS) and polystyrene (PS) coatings to protect the electronics of the magnetic sensors from the biological medium and to warrant optimal chemical and mechanical compliance of our device with the neural samples. The coatings were prepared separately from the sensors for experimental convenience, and spinal explants were cultured on top of them. The coatings were later fixed fully covering the magnetic sensors at the time of the measurements. In particular, organotypic spinal cord/dorsal root ganglia (DRG) slices obtained from E12–E13 mouse embryos, were grown on grooved PDMS and grooved PS films, as well as standard glass coverslips (control), for 2–3 weeks *in vitro* (see sketch in Fig. 1.A).

We selected PDMS and PS due to their well-established compatibility with the central nervous system [44,45]. In both polymeric coatings (50 μm thickness) grooves consisted of rectangular-profile micropatterns characterized by 20 μm pitch and 5 μm depth (Fig. 1.A). Such a design was deployed to favor the formation of spinal cord outgrowing bundles of axons and to control bundles direction, which in control samples, namely in the absence of patterns, is usually random (Fig. 1.B, Control).

Immunofluorescence microscopy was used to investigate the morphology and growth of spinal tissue explants and axons when interfaced to the different substrates. Fig. 1.B shows micrographs depicting at low magnification the entire spinal slice/DRG co-culture (top) and, at higher magnification, the appearance of axonal fiber bundles centrifugally growing from the slice (bottom) on the different substrates. In control spinal slices, without patterned interfaces, axons regrowth had no preferred orientation, with neurites usually organized centrifugally around the spinal tissue. Conversely, when the spinal cord slices (SCSs) were interfaced to patterned substrates (grooved PDMS and PS), an orientation of the regenerative axons was evident. We have measured the planar width and length of fiber bundles to quantify the impact of the substrate (see bar plots in Fig. 1.C). Fibers width was only slightly modified by anisotropic patterning (i.e., grooves), with a more prominent effect onto grooved PDMS substrates (394 ± 68 μm) than grooved PS or standard glass (respectively, 274 ± 56 μm and 184 ± 49 μm). On the other hand, neuronal fibers at the interface with grooves resulted in a greater bundles length (1350 ± 160 μm onto grooved PDMS and 1320 ± 170 μm onto grooved PS) compared to planar glass (470 ± 130

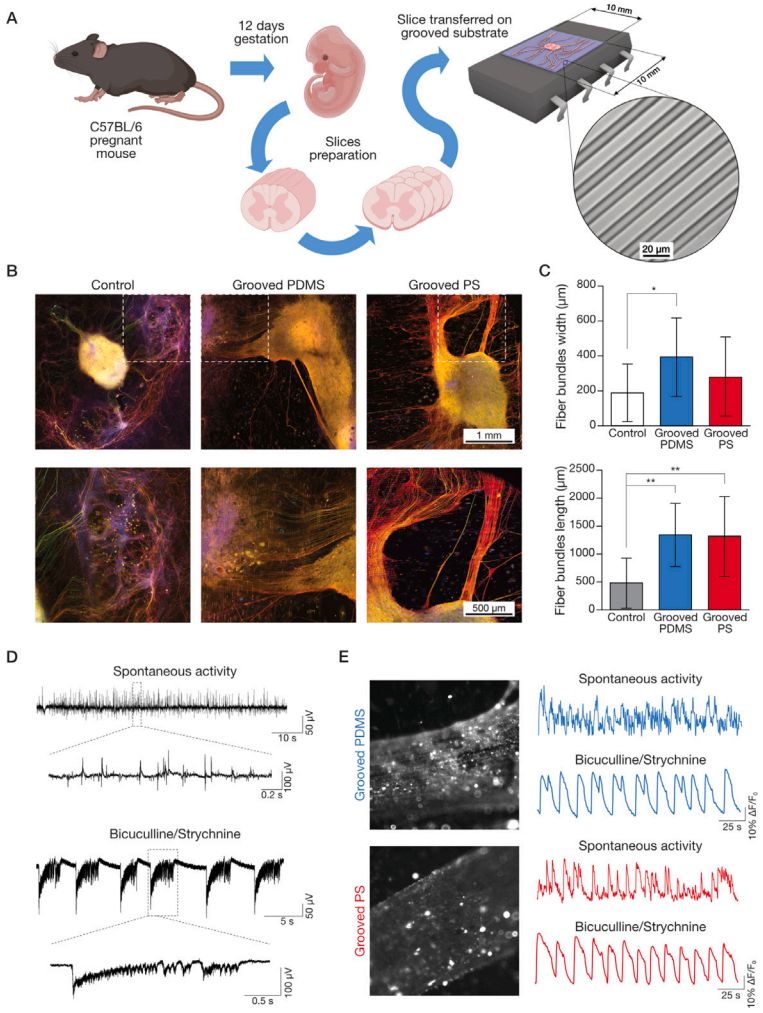

Fig. 1. Spinal cord organotypic cultures grown on PDMS or PS patterned substrates. (A) Sketch of the experimental design for culturing SCS on grooved coatings. The circular inset at the right shows a representative SEM magnification of a PDMS/PS micropatterned substrate in which the embossed linear grooves are visible. (B) Low (top) and high (bottom) magnification immunofluorescence micrographs of spinal cord cultures interfaced to control glass coverslip or to PDMS/PS coatings. Neurons are visualized with anti β-tubulin III (red), and with SMI-32 (green), while cell nuclei are targeted by DAPI (blue). (C) Bar plots summarize values of axon bundles width and length comparing the different substrates (m=6, from 3 independent cultures). (D) Extracellular recording sample traces in control spinal slice (spontaneous activity) and in the presence of blockers of synaptic inhibition (Bicuculline/Strychnine). (E) Snap-shots of spinal axon bundles on PDMS or PS grooved substrates labeled by Fluo-4 AM and fluorescence tracings in spontaneous activity and Bicuculline/Strychnine.

µm), making patterned surfaces preferable for our study and highly suitable for spinal axons targeted regrowth.

Cultured spinal explants and regrowing axons feature remarkable spontaneous electrical activity [46]. To further gain insight into the activity when detected at the level of projecting axons, we performed extracellular field potential recordings using low resistance (10 MΩ) glass micropipettes filled with extracellular saline solution. Recording electrodes were positioned in close proximity to the (visually identified) axon bundles and spontaneous activity of variable frequency and intensity, depending on the distance from and the size of the targeted bundle of axons, was recorded. An example of such recordings is given in Fig. 1.D (top tracings). We pharmacologically weaken synaptic inhibition by applying the glycine/γ-aminobutyric acid type A receptor antagonists strychnine (2 μM) and bicuculline (20 μM). As previously reported for spinal tissues [46] the weakening of inhibition promoted a switch from random bursting to synchrony, with the development of slow-paced bursting. This resulted in a rhythmic and periodic activity (Fig. 1.D, bottom tracings) of greater intensity and duration when compared with spontaneous activity. Therefore, we considered this protocol the best condition for sensing low magnetic fields at the axon bundles level.

Neuronal activity was also live recorded by Ca^{2+} dynamics fluorescence imaging (Fig. 1.E) [45]. Axons loaded with the membrane-permeable Ca^{2+}-dye Fluo-4 AM revealed typical spontaneous fluorescence increases detected in all fields recorded. When reducing inhibition, we measured the expected increase in signal rhythmicity and periodicity (Fig. 1.E. left, fluorescence tracings), in agreement to what observed in voltage recordings.

At the end of each experiment, either potential recordings or live calcium imaging, the voltage-gated Na^+ channel blocker Tetrodotoxin (TTX, 1 μM) was administrated to remove any action potential and impair synaptic activity, thus ensuring the neuronal nature of any recorded signals.

For the magnetic measurements (magnetophysiology), the PDMS/PS films supporting the spinal cord sample were directly placed on top of a TMR-based magnetic sensor, with the sensor axis perpendicular to the grooves of the films (i.e. to the grown axons), to record the magnetic signal without shielding (see Fig. 2.A) at room temperature. To avoid the background magnetic noise, we performed differential measurements using two TMR-based magnetic sensors, where the measuring sensor was placed at the smallest distance from the sample (~ 500 µm), and a secondary sensor was placed further apart (~ 1cm)

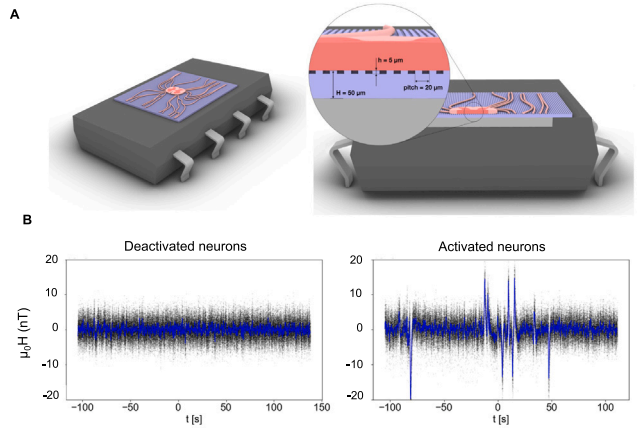

Fig. 2. Magnetophysiology measurements in organotypic SCSs. (a) The illustration shows the configuration of the experimental system. The pitch of the linear pattern was 20 μm, while the width and depth (h) of grooves were 10 μm and 5 μm, respectively. In the graphical representation, the total height of the micro-patterned substrate (H) is 50 μm and represents the distance between the encapsulation of the sensor and the organotypic preparation. (b) Real-time magnetic recording of the axonal activity pharmacological induced by bicuculline/strychnine and after inhibition by tetrodotoxin, validating the biological origin of the signal. The black dots correspond to raw data. Blue lines correspond to experimental data after filtering with a Butterworth low-pass filter. These lines have been incorporated as guides to the eye.

to subtracts the background noise. It is important to notice that the distance between the active part of the sensor and the sample is the thickness of the polymeric coating (~ 50 μm) and the encapsulation of the sensor. Additionally, a low noise electronic system was developed in order to amplify the small voltage signals keeping them undisturbed from electronic noise. Note that this configuration is different from that used in previous works [42] and it is key for the detection of real-time recordings. Fig. 2.B shows the output of the magnetic sensor setup with the neural tissue in the collective (low inhibition; Fig. 2) activation state, in which a sequence of peaks can be observed. In organotypic spinal slices, low inhibition state leads to neuronal outputs synchronous among all neurons [46]. The absence of any signal after TTX-removal of action potentials validates the source of the signal in the activation state as originating from the intrinsic biological sample's neural activity.

In order to have a real-time insight into the neural activity, we have combined magnetophysiology and live Ca^{2+} imaging. Fig. 3.A shows the output of the magnetic sensor with the neural tissue in the low inhibition activation state, in which a sequence of peaks can be observed. Simultaneous live Ca^{2+} imaging was recorded and provided additional evidence of the intrinsic biological origin of the magnetic signal. In fact, Fig. 3.A shows that the magnetophysiology peaks match perfectly with some of the Ca^{2+} imaging peaks. The absence of a one-to-one correlation between these recordings is expected. Indeed, the signal of the Ca^{2+} imaging was recorded from a visually selected field which was active at any bursts, while by magnetophysiology we detected only firing neurons close to the magnetic sensor. Moreover, the magnetic sensor is vectorial, and thus, it only detects the magnetic fields parallel to its measuring axis, while Ca^{2+} imaging is sensitive to all action potential propagation waves. This evidence is further sustained by Fig. 3.B, in which a time window was enlarged to show the match among the different signals clearly.

3. Conclusions

To sum up, we have performed in-vitro magnetic recordings of neural activity in organotypic SCSs obtained from mouse embryos. The magnetic recordings were performed in real time, with no magnetic shielding, applying no electrical excitation or stimulation, without any digital post-processing, nor using time-series averaging, reference-free, at room temperature, at distances far enough from the tissue to be noninvasive, using commercial sensors based on spin electronics. The magnetic recordings are corroborated by measurements using Ca^{2+} imaging, an extensively used technique in neurobiology. Moreover, the neural origin of the activity is further demonstrated by its inhibition using TTX pharmacology. It should be noted that, in magnetic detection, the secondary sensor is not used as a reference. Instead, it is employed to reduce noise and improve the signal-to-noise ratio through differential detection. This enables the detection of neural signals without requiring shielding or screening.

These results represent a step forward the development of portable and wearable device capable of detecting magnetic fields created by neuronal activity under practical conditions, which could allow the exploitation of the fundamental advantages of magnetophysiology to increase our understanding of neurobiology, developing it into a technique used every day much as the electrophysiology is today. Additionally, compared to the scalar nature of the electrophysiology recording, magnetic recordings would benefit from their vectorial nature, which would enable the identification of neural signal flow and, when combining different sensors, to estimate the 3D position of the neuronal sources. We envisage that future research should be focused on how magnetic recordings compare with well-established electrical recordings. Given the lower spatial resolution of magnetic sensors compared to implanted electrodes, it is essential to identify the specific new information that magnetophysiology can provide — distinct yet complementary to electrophysiology — in order to better integrate this technology into a new generation of neural interfaces. Addressing the challenge of clinical translation is also necessary.

4. Experimental details

4.1. Magnetic sensor and electronics

The magnetic sensors used in this work were TMR-based magnetic sensors from the TMR2922 series (Multidimension) with sensitivity in the range of 7–15 mV/V/Oe and typical detectivity of 1nT $Hz^{-1/2}$ at 1 Hz. The sensing element is mounted in a SOP8 package, ready for surface mounting. The conventional size for SOP8 package is $5.0 \times 6.0 \times 1.5$ mm^3. To avoid the background magnetic noise, we have performed differential measurements using two magnetic sensors. A working commercial sensor, encapsulated in PDMS or PS coatings to protect it from the biological medium, is placed close to the sample, at a distance shorter than 500 μm, whereas a secondary sensor is placed close to the measuring sensor (~1 cm). A low-noise electronic system has been developed in order to amplify the small voltage signals, keeping them undisturbed from electronic noise. The output of both sensors was independently amplified using low-noise operational amplifiers (INA217 for Texas Instruments) and then connected in differential mode using a third operational amplifier. Afterwards the signal was amplified by a commercial low noise amplifier SR560 (Standford Research Systems) that limited the bandwidth from 0.01 Hz up to 3 kHz. The overall gain is typically 1000. Finally, the signal is connected to a computer via a DAQ NI-USB 6356 (National Instruments).

4.2. Fabrication of micropatterned gratings for neuron aligned growth

To induce neuron alignment during growth, grating patterns on cell culture substrates were produced. The gratings were 5 μm in height and 10 μm in width, with periods of ca. 20 μm and were produced on PS and PDMS substrates.

To produce the PS films, a mold was initially fabricated by photolithography on photoresist (AZ9260) film with thicknesses ranging from 4.5 to 7 μm. Optical lithography was performed by using a maskless laser direct writing (Heidelberg DWL66). From the photopatterned

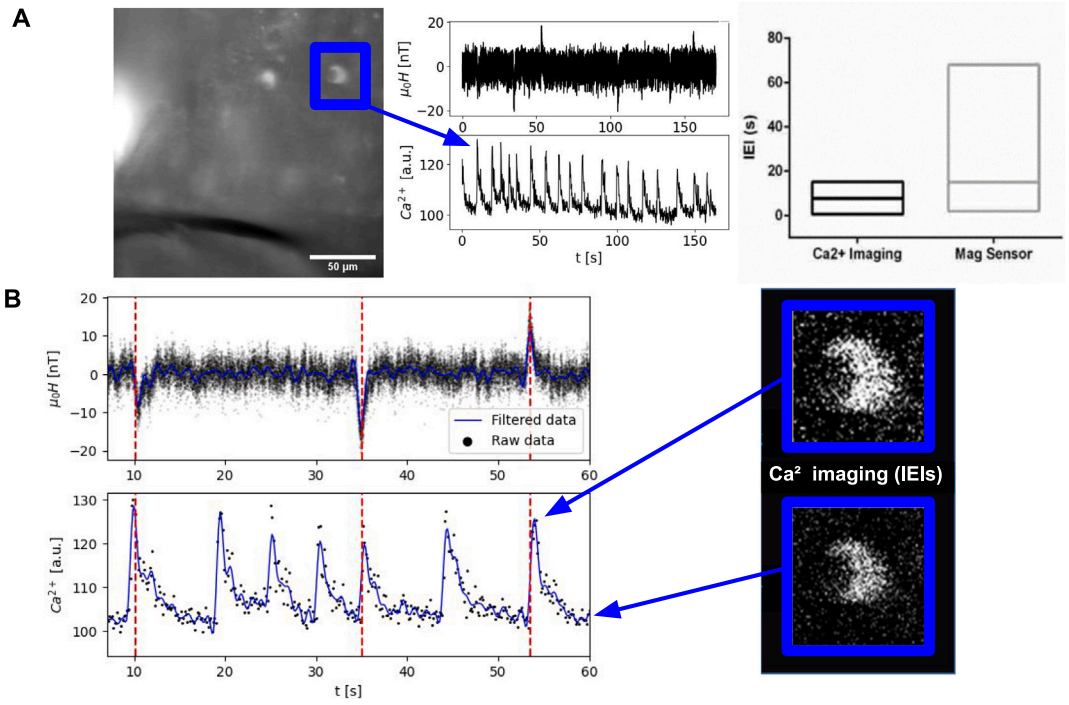

Fig. 3. Magnetic detection of neural activity corroborated with Ca^{2+} imaging. (A) Left: zoomed field of view in the ventral horn of a spinal cord organotypic slice loaded with Fluo4-AM during a Ca^{2+} imaging experiment performed simultaneously with magnetic sensor testing. Center: typical traces of Bic/Stryc-induced motor rhythm from a ventral horn neuron recorded simultaneously by Ca^{2+} imaging (top) and by magnetophysiology (bottom). The full experiment includes recording upon TTX administration which impairs action potential spreading along the axons. Right: Estimated inter-event intervals (IEIs) during pharmacologically Bic/Stryc -induced activity obtained in the Ca^{2+} imaging experiment and magnetophysiology (m=3). (B) Left: Selected traces by Ca^{2+} imaging and magnetophysiology at indicated time window. The black dots correspond to raw data. Blue lines correspond to experimental data after filtering with a Butterworth low-pass filter. These lines have been incorporated as guides to the eye. Right: Representative snapshots images at calcium bursts (top) and at rest (bottom).

substrate, PDMS replica was produced by casting the PDMS precursors (1:10 initiator) and curing at 70 °C for 1 h followed by 30 min at 130 °C before detaching it. One important constraint for this fabrication was producing as thin substrates as possible, below 200 μm, for the neuron activity sensing experiments. To obtain such thin substrates, the PS films were prepared by solution casting of 10% PS toluene solution. Upon solvent evaporation, the films were peeled off from the carrier and imprinted to produce the micron patterned gratings. The nanoimprint conditions were (T = 130 °C; P = 30 bar and t = 5 min).

To fabricate the PDMS grating on 50–100 μm thin films, the PDMS replica substrate was imprinted into an intermediate thermoplastic commercial material with very low surface energy (Intermediate Polymer Stamp - Obducat). Then, an amount of PDMS was deposited on a Petri dish and the IPS grating replica film was placed upside down. The PDMS was cured using the same protocol as above. After detachment, a PDMS micropatterned free-standing film was obtained. To produce PDMS patterned films with thickness ranging 10–20 μm on thin cover slips, initially, PDMS replica substrate was spin coated over the IPS micropatterned substrate (2000 rpm, 1 min). Then, a glass coverslip (12 × 24 mm^2) was placed on top and the PDMS was cured. After curing, the IPS substrate was peeled off, and the PDMS patterned film remained attached to the glass. Both PS and PDMS-made grooved substrates have been prepared with lateral dimensions ranging from 12 × 24 to 20 × 20 mm^2. Subsequently, small square pieces of about 10 × 10 mm^2 were cut out. Organotypic slices were placed and cultured above such samples.

4.3. Organotypic slice cultures

Spinal cord/dorsal root ganglia (DRG) slices were obtained from embryos at 12–13 days of gestation (E12–E13) from a pregnant mouse (C57Bl/6), as previously reported [47]. All procedures were approved by the local veterinary authorities and performed in accordance with the Italian law (decree 26/14) and the UE guidelines (2007/526/CE and 2010/63/UE). The animal use was approved by the Italian Ministry of Health (22DABN1WO). All efforts were made to minimize suffering and to reduce the number of animals used. Pregnant mice were terminated by CO_2 overdose and subsequent decapitation, while fetuses were extracted by cesarean section. The thoracolumbar extent of their spinal cord was transected and cut into transversal slices (275 μm) with a tissue chopper (McIlwain TC752, Campden Instruments Ltd.). Slices were dissected from the surrounding tissue and plated onto either standard glass coverslips or onto micropatterned PS and PDMS substrates by clotting 15 μL of chicken plasma with 23 μL of thrombin (both from Sigma-Aldrich). Organotypic Spinal Cords were therefore grown with 1 mL medium containing 66% DMEM 1x (Gibco), 8% sterile water for tissue culture, 25% fetal bovine serum (Gibco), 1% antibiotic-antimycotic (Gibco), 2% B-27 supplement (Gibco) and 20 ng/mL nerve growth factor (NGF, Alomone Laboratories); 300 mOsm; pH 7.35. Cultures were kept in a roller drum (120 revs/min, at 37 °C and 5% CO_2). After 7 DIV, culture medium was replaced for 24 h by fresh medium containing antimitotics (10 μM ARA-C/Uridine/5-Fl-dU) and reduced NGF concentration (5 ng/mL). At DIV 8, fresh medium with reduced NGF was added and refreshed every 7 days. All the electrophysiological experiments have been conducted at DIV 14–16 on samples from 3 different organotypic preparations.

4.4. Organotypic culture immunofluorescence and confocal microscopy

Organotypic slices were fixed in 4% formaldehyde, prepared from fresh paraformaldehyde, in PBS 1x for at least 1 h. After fixation, slices were incubated for 10 min with 0.1 M glycine in PBS 1x and permeabilized for 1 h with 0.3% Triton-X-100 (Carlo Erba) in PBS added with 5% FBS (Gibco) and 4% BSA (Sigma-Aldrich) to prevent non-specific

binding of primary antibodies. Samples were subsequently incubated 4 h with primary antibodies and 1 h with the secondary antibodies, both at 37 °C in a humidified incubator (three washes in PBS 1x preceded each step). Mounting was performed with anti-fade medium Fluoromount (Sigma-Aldrich) on 1 mm thick microscope glass slides. All neurons were labeled through anti-β-tubulin III primary antibody (1:800, Sigma-Aldrich) and visualized with Alexa 594 anti-rabbit in goat as the secondary antibody (1:800, Invitrogen). Exclusive staining of motoneurons and DRG was instead achieved with anti-neurofilament H (SMI-32, 1:800, Biolegend) recognized by Alexa 488 anti-mouse in goat as the secondary antibody (1:800, Invitrogen). Nuclei were stained with 4,6-diamidino-2-phenylindole (DAPI, 1:500, Invitrogen). The motorized xy scanning module of an Eclipse Ti2 inverted A1R system (Nikon Instruments) was used to acquire stitched images (10x Plan Apo λ, 0.45 NA) to obtain a morphological insight of the stained spinal cord slice cultures. Planar width and length of fiber bundles were quantified by analyzing 6 fields of view per condition with ImageJ software (NIH).

4.5. Electrophysiological recordings

Organotypic spinal explants were placed on an upright microscope Eclipse FN1 (Nikon Instruments). Cultures were continuously perfused at 5 mL/min rate and room temperature with an extracellular saline solution of composition (mM): 150 NaCl, 4 KCl, 2 $CaCl_2$, 1 $MgCl_2$, 10 HEPES, 10 glucose (pH adjusted to 7.4 with NaOH; osmolarity 300 mOsm). Extracellular recordings of axon-bundles were obtained using an Ag/AgCl electrode inserted in a borosilicate glass micropipettes (10 MΩ) filled with the same extracellular saline as above. Neural signals were amplified by a Multiclamp 700B patch amplifier (Axon Instruments, Molecular Devices LLC, US) and data were collected and digitized at a sampling rate of 20 kHz (10 kHz lowpass filtered) using a Digidata 1322 A (Axon Instruments, Molecular Devices LLC, US). After spontaneous activity monitoring, 25 μM bicuculline ($GABA_A$ receptor antagonist; Sigma-Aldrich) and 2 μM strychnine (glycine receptor antagonist; Sigma-Aldrich) were perfused to disinhibit the network and produce long-lasting bursts of summating action potentials. In all experiments, at the end 1 μM TTX (a voltage-gated, fast Na^+ channel blocker; Latoxan) was added to assess the neuronal origin of recorded signals.

4.6. Calcium imaging

Organotypic spinal slices were loaded with cell-permeable Ca^{2+} dye Fluo-4 AM (Molecular Probes); briefly, 11.6 μL of DMSO (Sigma-Aldrich) were added to the stock 50 μg of the dye, and cultures were incubated with a final concentration of 4 μM for 1 h in the roller drum incubator at 37 °C, 5% CO_2. Dye loading was followed by a 20 minutes-long de-esterification step in extracellular saline solution (see above). Samples were mounted either on an upright microscope Eclipse FN1 (Nikon Instruments) equipped with a Andor iXon Ultra 897 EM-CCD (Oxford Instruments) or on an inverted Eclipse Ti-U (Nikon Instruments) equipped with an ORCA-Flash4.0 V2 sCMOS (Hamamatsu) operating at binning 4. Cultures were continuously perfused at 5 mL/min rate and room temperature with the above-described extracellular saline solution. The Ca^{2+} dye was excited at 488 nm, emitted light passed to a 490 nm dichroic and was further filtered to 520 nm. Activity was monitored either with a 40x objective (PlanFluor, 0.75 NA) or a 40x water immersion objective (Fluor, 0.80 NA). Images were acquired every 150 ms. After cultures accustomed to the extracellular solution, spontaneous activity was recorded for 10 min. In all experiments, at the end 1 μM TTX (a voltage-gated, fast Na^+ channel blocker; Latoxan) was added to assess the neuronal origin of recorded signals. Images were analyzed with ImageJ software (NIH), and the corresponding calcium traces were extracted with Clampfit software (pClamp suite, 10.4 version; Axon Instruments) in off-line.

4.7. Statistical analysis

Statistical analysis was accomplished using Prism 6 software (GraphPad): data sets normality was addressed with D'Agostino and Pearson omnibus normality test. Non-parametric tests were used in both non-normally distributed data and unequal variances among tested data sets. Accordingly, statistics between two independent samples were performed with t-test or Mann–Whitney U test. In contrast, three independent samples differences were tested with either one-way ANOVA adjusted for multiple comparisons with Tukey's correction or Kruskal–Wallis test adjusted with Dunn's multiple comparison test. Calcium and magnetic events were analyzed using the inter-event interval (IEI) parameter, which measures the period between successive signal peaks, particularly informative when the detected activity is irregular (i.e., when bursts of activity are present) or occurring at a low pace. All data are plotted as median with their 25th (1st quartile, Q1) and 75th (3rd quartile, Q3) percentiles, with whiskers representing 10th and 90th percentiles. Descriptive statistics used in the text express the central tendency as mean ± SD for normal distributions and median for non-normal distributions. All experiments have been conducted on $n \geq 3$ samples from at least 3 independent experimental sessions (i.e. organotypic slice culture preparations.

CRediT authorship contribution statement

Arturo Vera: Investigation, Formal analysis. **Ivo Calaresu:** Investigation, Formal analysis. **Isidoro Martínez:** Software, Investigation, Formal analysis. **Rubén Guerrero:** Supervision, Software, Investigation, Formal analysis. **Denis Scaini:** Methodology, Investigation, Formal analysis. **Guillermo de Arana Schoebel:** Formal analysis. **Jaime J. Hernandez:** Investigation. **Isabel Rodríguez:** Writing – review & editing, Supervision, Project administration, Methodology, Investigation. **Rodolfo Miranda:** Supervision, Funding acquisition. **Eduardo Daniel Martín:** Resources, Investigation. **Julio Camarero:** Writing – review & editing, Resources, Methodology, Funding acquisition, Conceptualization. **María Teresa González:** Writing – review & editing, Supervision, Project administration, Methodology, Funding acquisition, Conceptualization. **Lucas Pérez:** Writing – original draft, Supervision, Resources, Methodology, Investigation, Conceptualization. **Laura Ballerini:** Writing – original draft, Supervision, Resources, Investigation, Funding acquisition, Conceptualization.

Declaration of competing interest

The authors declare that they have no known competing financial interests or personal relationships that could have appeared to influence the work reported in this paper.

Acknowledgments

This work was funded by the European Union's Horizon 2020 research and innovation programme under Grant agreement No. 737116 (ByAxon project) and agreement No. 101169352 (MSCA Doctoral Network programme NeuroNanotech), and by the Spanish MICINN under projects NEURALFLEX (PID2023-153180OB-I00), NanoScell (PDC2021-121515 I00) and the 'Severo Ochoa' Programme for Centres of Excellence in R&D (CEX2020-001039-S), as well as the Comunidad de Madrid through the project TEC-2024/TEC-380 "Mag4TIC".

Appendix A. Supplementary data

Supplementary material related to this article can be found online at https://doi.org/10.1016/j.sbsr.2025.100885.

Data availability

Data will be made available on request.

References

[1] C. Pizzolato, M.A. Gunduz, D. Palipana, J. Wu, G. Grant, S. Hall, R. Dennison, R.D. Zafonte, D.G. Lloyd, Y.D. Teng, Non-invasive approaches to functional recovery after spinal cord injury: Therapeutic targets and multimodal device interventions, Exp. Neurol. 339 (2021) 113612.

[2] W. Yang, R. Yuste, In vivo imaging of neural activity, Nat. Methods 14 (2017) 349–359.

[3] J. Wu, Y. Liang, S. Chen, C.-L. Hsu, M. Chavarha, S.W. Evans, D. Shi, M.Z. Lin, K.K. Tsia, N. Ji, Kilohertz two-photon fluorescence microscopy imaging of neural activity in vivo, Nat. Methods 17 (2020) 287–290.

[4] G. Hong, C.M. Lieber, Novel electrode technologies for neural recordings, Nat. Rev. Neurosci. 20 (2019) 330–345.

[5] N.B. Standen, P.T.A. Gray, M.J. Whitaker. (Eds.), Microelectrode Techniques: The Plymouth Workshop Handbook, The Company of Biologists Limited, Cambridge, 1987.

[6] G. Buzsáki, C.A. Anastassiou, C. Koch, The origin of extracellular fields and currents - EEG, ecog, LFP and spikes, Nat. Rev. Neurosci. 13 (2012) 407–420.

[7] J.L. Collinger, S. Foldes, T.M. Bruns, B. Wodlinger, R. Gaunt, D.J. Weber, Neuroprosthetic technology for individuals with spinal cord injury, J. Spinal Cord. Med. 36 (2013) 258–272.

[8] D.R. Gater Jr., D. Dolbow, B. Tsui, A.S. Gorgey, Functional electrical stimulation therapies after spinal cord injury, NeuroRehabilitation 28 (2012) 231–248.

[9] A. Rowald, S. Komi, R. Demesmaeker, E. Baaklini, S.D. Hernandez-Charpak, E. Paoles, H. Montanaro, A. Cassara, F. Becce, B. Lloyd, T. Newton, J. Ravier, N. Kinany, M. D'Ercole, A. Paley, N. Hankov, C. Varescon, L. McCracken, M. Vat, M. Caban, A. Watrin, C. Jacquet, L. Bole-Feysot, C. Harte, H. Lorach, A. Galvez, M. Tschopp, N. Herrmann, M. Wacker, L. Geernaert, I. Fodor, V. Radevich, K.V.D. Keybus, G. Eberle, E. Pralong, M. Roulet, J.-B. Ledoux, E. Fornari, S. Mandija, L. Mattera, R. Martuzzi, B. Nazarian, S. Benkler, S. Callegari, N. Greiner, B. Fuhrer, M. Froeling, N. Buse, T. Denison, R. Buschman, C. Wende, D. Ganty, J. Bakker, V. Delattre, H. Lambert, K. Minassian, C.A.T. van den Berg, A. Kavounoudias, S. Micera, D.V.D. Ville, Q. Barraud, E. Kurt, N. Kuster, E. Neufeld, M. Capogrosso, L. Asboth, F.B. Wagner, J. Bloch, G. Courtine, Activity-dependent spinal cord neuromodulation rapidly restores trunk and leg motor functions after complete paralysis, Nat. Med. 28 (2022) 260–271.

[10] M.A. Lebedev, M.A.L. Nicolelis, Brain-machine interfaces: past, present and future, Trends. Neurosci. 29 (2006) 536–546.

[11] J.J. Shih, D.J. Krusienski, J.R. Wolpaw, Brain-computer interfaces in medicine, Mayo Clin. Proc. 87 (2012) 268–279.

[12] J.L. Collinger, B. Wodlinger, J.E. Downey, W. Wang, E.C. Tyler-Kabara, D.J. Weber, A.J.C. McMorland, M. Velliste, M.L. Boninger, A.B. Schwartz, High-performance neuroprosthetic control by an individual with tetraplegia, Lancet 381 (2013) 557–564.

[13] A.B. Ajiboye, F.R. Willett, D.R. Young, W.D. Memberg, B.A. Murphy, J.P. Miller, B.L. Walter, J.A. Sweet, H.A. Hoyen, M.W. Keith, P.H. Peckham, J.D. Simeral, J.P. Donoghue, L.R. Hochberg, R.F. Kirsch, Restoration of reaching and grasping movements through brain-controlled muscle stimulation in a person with tetraplegia: a proof-of-concept demonstration, Lancet 389 (2017) 1821–1830.

[14] C.E. Bouton, A. Shaikhouni, N.V. Annetta, M.A. Bockbrader, D.A. Friedenberg, D.M. Nielson, G. Sharma, P.B. Sederberg, B.C. Glenn, W.J. Mysiw, A.G. Morgan, M. Deogaonkar, A.R. Rezai, Restoring cortical control of functional movement in a human with quadriplegia, Nature 533 (2017) 247–250.

[15] J.A. Herron, M.C. Thompson, T. Brown, H.J. Chizeck, J.G. Ojemann, A.L. Ko, Cortical brain-computer interface for closed-loop deep brain stimulation, IEEE Trans. Neural. Syst. Rehabil. Eng. 25 (2017) 2180–2187.

[16] J.W. Salatino, K.A. Ludwig, T.D.Y. Kozai, E.K. Purcell, Glial responses to implanted electrodes in the brain, Nat. Biomed. Eng. 1 (2017) 862–877.

[17] J.C. Barrese, N. Rao, K. Paroo, C. Triebwasser, C. Vargas-Irwin, L. Franquemont, J.P. Donoghue, Failure mode analysis of silicon-based intracortical microelectrode arrays in non-human primates, J. Neural Eng. 10 (2013) 066014.

[18] G. Rios, E.V. Lubenov, D. Chi, M.L. Roukes, A.G. Siapas, Nanofabricated neural probes for dense 3-D recordings of brain activity, Nano Lett 16 (2016) 6857–6862.

[19] Y. Wu, H. Chen, L. Guo, Opportunities and dilemmas of in vitro nano neural electrodes, RSC Adv. 10 (2020) 187–200.

[20] J.J. Jun, N.A. Steinmetz, J.H. Siegle, D.J. Denman, M. Bauza, B. Barbarits, A.K. Lee, C.A. Anastassiou, A. Andrei, C. Aydin, M. Barbic, T.J. Blanche, V. Bonin, J. Couto, B. Dutta, S.L. Gratiy, D.A. Gutnisky, M. Häusser, B. Karsh, P. Ledochowitsch, C.M. Lopez, C. Mitelut, S. Musa, M. Okun, M. Pachitariu, J. Putzeys, P.D. Rich, C. Rossant, W. lung Sun, K. Svoboda, M. Carandini, K.D. Harris, C. Koch, J. O'Keefe, T.D. Harris, Fully integrated silicon probes for high-density recording of neural activity, Nature 551 (2017) 232–236.

[21] T. Stieglitz, H. Beutel, M. Schuettler, J.U. Meyer, Micromachined, polyimide-based devices for flexible neural interfaces, Biomed. Microdevices 2 (2000) 283.

[22] M. Vomero, F. Ciarpella, E. Zucchini, M. Kirsch, L. Fadiga, T. Stieglitz, M. Asplund, On the longevity of flexible neural interfaces: Establishing biostability of polyimide-based intracortical implants, Biomaterials 281 (2022) 121372.

[23] F. Wu, L.W. Tien, F. Chen, J.D. Berke, D.L. Kaplan, E. Yoon, Silk-backed structural optimization of high-density flexible intracortical neural probes, J. Microelectromech. Syst. 24 (2015) 62–69.

[24] H. Cui, X. Xie, S. Xu, L.L.H. Chan, Y. Hu, Electrochemical characteristics of microelectrode designed for electrical stimulation, BioMed. Eng. OnLine 18 (2019) 86.

[25] C. Cointe, A. Laborde, L.G. Nowak, D.N. Arvanitis, D. Bourrier, C. Bergaud, A. Maziz, Scalable batch fabrication of ultrathin flexible neural probes using a bioresorbable silk layer, Microsyst Nanoeng. 8 (2022) 21.

[26] M. Ganji, A. Tanaka, V. Gilja, E. Halgren, S.A. Dayeh, Scaling effects on the electrochemical stimulation performance of au, pt, and PEDOT:PSS electrocorticography arrays, Adv. Funct. Mater. 27 (2017) 1703019.

[27] A. Altuna, J. Berganzo, L.J. Fernández, Polymer SU-8-based microprobes for neural recording and drug delivery, Front. Mater. 2 (2015) 47.

[28] C. Böhler, M. Vomero, M. Soula, M. Vöröslakos, M. Porto Cruz, R. Liljemalm, G. Buzsaki, T. Stieglitz, M. Asplund, Multilayer arrays for neurotechnology applications (MANTA): Chronically stable thin-film intracortical implants, Adv. Sci. 10 (14) (2023) 2207576.

[29] T. Stieglitz, M. Schuettler, B. Rubehn, T. Boretius, J. Badia, X. Navarro, Evaluation of polyimide as substrate material for electrodes to interface the peripheral nervous system, in: 2011 5th International IEEE/EMBS Conference on Neural Engineering, 2011, pp. 529–533.

[30] M. Ganji, E. Kaestner, J. Hermiz, N. Rogers, A. Tanaka, D. Cleary, S.H. Lee, J. Snider, M. Halgren, G.R. Cosgrove, B.S. Carter, D. Barba, I. Uguz, G.G. Malliaras, S.S. Cash, V. Gilja, E. Halgren, S.A. Dayeh, Development and translation of PEDOT:PSS microelectrodes for intraoperative monitoring, Adv. Funct. Mater. 28 (12) (2018) 1700232.

[31] J.E. Chung, H.R. Joo, J.L. Fan, D.F. Liu, A.H. Barnett, S. Chen, C. Geaghan-Breiner, M.P. Karlsson, M. Karlsson, K.Y. Lee, H. Liang, J.F. Magland, J.A. Pebbles, A.C. Tooker, L.F. Greengard, V.M. Tolosa, L.M. Frank, High-density, long-lasting, and multi-region electrophysiological recordings using polymer electrode arrays, Neuron. 101 (2019) 21–31.

[32] L. Luan, X. Wei, Z. Zhao, J.J. Siegel, O. Potnis, C.A. Tuppen, S. Lin, S. Kazmi, R.A. Fowler, S. Holloway, A.K. Dunn, R. A.Chitwood, C. Xie, Ultraflexible nanoelectronic probes form reliable, glial scar-free neural integration, Sci. Adv. 3 (2017) e1601966.

[33] J. Schulte, D. Ashouri, T. Stieglitz, The longevity of neural interfaces - mechanical oscillation of thin film metal-based neural electrodes determine stability during electrical stimulation, Adv. Func. Mater. 34 (11) (2024) 2310130.

[34] D. Scaini, L. Ballerini, Nanomaterials at the neural interface, Curr. Opin. Neurobiol. 50 (2018) 50–55.

[35] E. Lestrell, C.M. O'Brien, R. Elnathan, N.H. Voelcker, Vertically aligned nanostructured topographies for human neural stem cell differentiation and neuronal cell interrogation, Adv. Ther. 4 (9) (2021) 2100061.

[36] S.M. Wellman, J.R. Eles, K.A. Ludwig, J.P. Seymour, N.J. Michelson, W.E. McFadden, A.L. Vazquez, T.D.Y. Kozai, A materials roadmap to functional neural interface design, Adv. Func. Mater. 28 (12) (2018) 1701269.

[37] J.P. Wikswo, Biomagnetic sources and their models, in: S.J. Williamson, M. Hoke, G. Stroink, M. Kotani (Eds.), Advances in Biomagnetism, Springer US, Boston, MA, 1989, pp. 1–18.

[38] D. Cohen, Magnetoencephalography: Detection of the brain's electrical activity with a superconducting magnetometer, Science 175 (1972) 664–666.

[39] M. Proudfoot, M.W. Woolrich, A.C. Nobre, M.R. Turner, Magnetoencephalography, Pr. Neurol. 14 (2014) 336–343.

[40] E. Boto, N. Holmes, J. Leggett, G. Roberts, V. Shah, S.S. Meyer, L.D. Munoz, K.J. Mullinger, T.M. Tierney, S. Bestmann, G.R. Barnes, R. Bowtell, M.J. Brookes, Moving magnetoencephalography towards real-world applications with a wearable system, Nature 555 (2018) 657–661.

[41] R. Zhang, W. Xiao, Y. Ding, Y. Feng, X. Peng, L. Shen, C. Sun, T. Wu, Y. Wu, Y. Yang, Z. Zheng, X. Zhang, J. Chen, H. Guo, Recording brain activities in unshielded earth's field with optically pumped atomic magnetometers, Sci. Adv. 6 (2020) eaba879.

[42] L. Caruso, T. Wunderle, C.M. Lewis, J. Valadeiro, V. Trauchessec, J.T. Rosillo, J.P. Amaral, J. Ni, P. Jendritza, C. Fermon, S. Cardoso, P.P. Freitas, P. Fries, M. Pannetier-Lecoeur, In vivo magnetic recording of neuronal activity, Neuron. 95 (2017) 1283–1291.

[43] R. Sapkota, S. Isik, H. Suyanto, N.N. Rupiasih, N. Ingles, C. Rizal, Sensor with combined plasmonic and magnetic activities, Biosens. Bioelectron.: X 19 (2024) 100506.

[44] A. Vera, I. Martínez, L.G. Enger, B. Guillet, R. Guerrero, J.M. Diez, O. Rousseau, M. Lam Chok Sing, V. Pierron, P. Perna, J.J. Hernández, I. Rodríguez, I. Calaresu, A. Meier, C. Huck, A. Domínguez-Bajo, A. González-Mayorga, E. López-Dolado, M.C. Serrano, L. Ballerini, L. Pérez, R. Miranda, S. Flament, M.T. González, L. Mechin, J. Camarero, High-performance implantable sensors based on anisotropic magnetoresistive $La_{0.67}Sr_{0.33}MnO_3$ for biomedical applications, ACS Biomater. Sci. Eng 9 (2) (2023) 1020–1029.

[45] I. Calaresu, J. Hernandez, R. Rauti, B.L. Rodilla, A. Arché-Núñez, L. Perez, J. Camarero, R. Miranda, M.T. González, I. Rodríguez, D. Scaini, L. Ballerini, Polystyrene nanopillars with inbuilt carbon nanotubes enable synaptic modulation and stimulation in interfaced neuronal networks, Adv. Mater. Interfaces 8 (9) (2021) 2002121.

[46] S. Usmani, E.R. Aurand, M. Medelin, A. Fabbro, D. Scaini, J. Laishram, F.B. Rosselli, A. Ansuini, D. Zoccolan, M. Scarselli, M.D. Crescenzi, S. Bosi, M. Prato, L. Ballerini, 3D meshes of carbon nanotubes guide functional reconnection of segregated spinal explants, Sci. Adv. 2 (7) (2016) e1600087.

[47] D. Avossa, M.D. Rosato-Siri, F. Mazzarol, L. Ballerini, Spinal circuits formation: a study of developmentally regulated markers in organotypic cultures of embryonic mouse spinal cord, Neurosci. 122 (2003) 391–405.